

Molecular dynamics study of particle–particle collisions between hydrogen-passivated silicon nanoparticles

T. Hawa and M. R. Zachariah*

Center for NanoEnergetics Research, Departments of Mechanical Engineering and Chemistry, University of Minnesota, Minneapolis, Minnesota 55455, USA

(Received 20 January 2003; revised manuscript received 14 July 2003; published 30 January 2004)

One of the significant challenges in the use of nanoparticles is the control of primary particle size and extent of agglomeration when grown from the gas phase. In this paper we evaluate a possible strategy of surface passivation. Here the particle–particle interaction of hydrogen-surface-terminated silicon nanoparticles has been evaluated using molecular dynamics simulation. Nanoparticles of the size between 200 and 6400 silicon atoms at 300–1800 K were studied with a reparametrized Kohen-Tully-Stillinger empirical interatomic potential. A hydrogen monolayer is shown to prevent coalescence between particles under thermal collision conditions. The critical approach energy for coalescence was found to increase with increasing particle size but decreases with increasing temperature. Both solid and liquid droplets were seen to bounce at thermal energies, and in some cases, “superelastic” collisions are observed, where the rebound kinetic energy of the droplet is higher than the approach energy. These results suggest that surface coatings can significantly retard nanoaerosol growth.

DOI: 10.1103/PhysRevB.69.035417

PACS number(s): 61.46.+w, 61.20.Ja

I. INTRODUCTION

Fabrication of nanometer particles in both large quantities and at a sufficiently low cost has been considered one of the major challenges for their applications in microelectronics and advanced materials. Preparation of these materials at the industrial scale by vapor-phase condensation usually involves rapid coagulation due to the high concentrations used. In addition, the rate of collision and subsequent coalescence of particles determines the size of the spherical primary particles and the growth of agglomerates. A schematic of nanoparticle growth in a gas-phase process is shown in Fig. 1. An aerosol model that purports to represent the growth and shape of particles must have within it the basic physics behind the coalescence process.¹ Depending on the desired end use of the particles, different primary particle sizes and extents of agglomeration are desired. In many cases the main focus is towards minimizing agglomeration (Xiong and Pratsinis²), while, for example, for new classes of energetic materials, the main focus is to maximize agglomeration so as to increase the exposed surface area of the particles available for reaction. In the end the nature of the final primary particle size, and the extent of agglomeration are determined by the competition between the time for particle–particle collisions and coalescence. If the characteristic collision time between particles is less than the characteristic coalescence time, particles will coalesce before another collision event occurs. However, if the collision time is less than the characteristic coalescence time, chain aggregates result:

$$\tau_{\text{coalescence}} < \tau_{\text{collision}} \rightarrow \text{spherical particle,}$$

$$\tau_{\text{coalescence}} > \tau_{\text{collision}} \rightarrow \text{agglomerate.}$$

Conceptually then we can control particle morphology and size by either controlling the characteristic coalescence time or the collision time. Obviously one simple method to

change collision time is by changing the number concentration of nanoparticles, but controlling the characteristic coalescence time is more challenging because of the nonlinear nature of the coalescence dependence on temperature.

For example, the characteristic coalescence time calculated from a solid-state diffusion model is written as^{3–6}

$$\tau_f = \frac{3kT_p N}{64\pi\sigma D}, \quad (1)$$

where T_p is the particle temperature, N is the number concentration, D is the solid-state diffusion coefficient reported as an Arrhenius function of the temperature,⁷ and σ is the surface tension of the particle. For viscous flow, the coalescence time is given by

$$\tau_f = \frac{\eta d_p}{\sigma}, \quad (2)$$

where d_p is the diameter of the particle and η is the temperature-dependent viscosity.⁸ Zachariah and Carrier⁹ re-

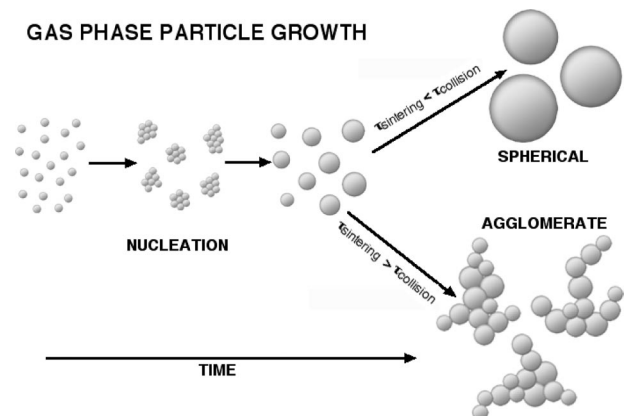


FIG. 1. Temporal evolution of vapor-phase particle growth.

ported the kinetics of growth and coalescence of silicon nanoparticles using molecular dynamics (MD) calculations. They reported that the particle morphology and the coalescence time are very sensitive to particle temperature and that the coalescence time also depends on particle size for solid-like particles.

In the consideration above it is always assumed that the all collisions lead to either agglomeration and/or coalescence. However, one might argue that another approach would be to change the surface properties of particles such that not all collisions are reactive or that somehow the coalescence rate could be altered by surface functionalization. The purpose of this paper is to investigate this possibility using computational modeling. We choose hydrogen passivation of silicon as our test system to investigate the effect on surface reactivity.

Background on surface reactivity

Recent classical MD studies by Ramalingam, Maroudas, and Aydil¹⁰ and Ohira, Ukai, and Noda¹¹ demonstrated that the presence of a hydrogen monolayer on the flat surface of silicon changes the reactivity of SiH_x ($0 \leq x < 4$) radicals with the surface significantly. They also found good agreement between the average reaction probability and experimental data.

These studies suggested to us a third approach to control the growth of particles using the presence of a hydrogen monolayer on the surface of a silicon particle. It is well known that silicon grown from silane and silicon in the presence of hydrogen show significant amounts of surface hydrogen.^{12,13} Onischuk *et al.* investigated the mechanism of aerosol formation during thermal decomposition of silane and found that during the initial stage of particle growth, hydrogen is mainly contained in polysilane chains formed in turn by pyrolysis products with a stoichiometry of Si_nH_{2n} .¹⁴ During later stages the particles are formed from hydrogen-depleted intermediates, and the hydrogen in particles is mainly bound in monohydride groups. It is therefore quite conceivable that one could produce such materials from vapor.

A number of mathematical models have been proposed to study particle bounce for micron-sized bodies or larger. The contact between two smooth elastic bodies was investigated by Hertz,¹⁵ who demonstrated that both the size and shape of the zone of contact followed from elastic deformation. Johnson, Kendall, and Roberts¹⁶ suggested that at zero applied load, the radius of the contact area made by an attractive interaction of two spherical particles of the same size is given by

$$a_0 = R(6\Gamma\pi R)/K,$$

where Γ is the energy per unit contact area, $R = R_0/2$, and $K = 8\pi k/3$. R_0 is the radius of the particle and k is the elastic constant of the material, i.e., $k = (1 - \nu)/(\pi E)$, where ν is the Poisson ratio and E the Young modulus of the particle. This theory implies that the contact area is proportional to the number of atoms to the $\frac{4}{3}$ th power.

We note that pure silicon particles would attract each other, while the hydrogen monolayer creates repulsive forces between the particles. To our knowledge, there is no simple contact mechanics theory for particles with heterogeneous layers. Also, to our knowledge this approach has never been investigated either by experiment or theory/simulation. We have chosen to employ molecular dynamics (MD) simulation, because of our prior use of the method to study the coalescence rate of bare silicon nanoparticles. The use of MD allows us, in a very systematic manner, to study the role of the passivating layer as a function of particle size, temperature, and collision energy. In this paper we limit our investigation to the particle–particle collision event (reactivity), and leave the issue of the role of surface passivation on coalescence rate to a subsequent paper.

II. COMPUTATIONAL MODEL

This study involves atomistic simulations using classical molecular dynamics. For this study we have modified the interatomic potential for silicon developed by Stillinger and Weber¹⁷ (SW) and extended by Kohen, Tulley, and Stillinger¹⁸ (KTS) to include Si-H and H-H interactions. Similar sets of potential energy functions have also been developed by Murty and Atwater,¹⁹ Ohira *et al.*,^{11,20,21} and Ramalingam, Maroudas, and Aydil,¹⁰ where a Tersoff-type potential^{22–25} was extended to describe interatomic interactions in the Si:H system. This extended version of the Tersoff potential has been tested successfully for its accuracy in describing the Si:H system in several earlier studies; however, the simulation of liquid silicon was not well described by the potential.²⁴ By contrast, the extended SW potential (KTS) was designed to describe interactions in both solid and liquid forms of silicon, and while it is known that the SW potential does not give accurate structures for very small (< 15 atoms) Si clusters at 0 K,^{26,27} it produces the correct structure for bulk liquid Si.²⁸ We have chosen to use the KTS potential since most synthesis processes leading to cluster formation occur at high temperature, cluster growth by coalescence is

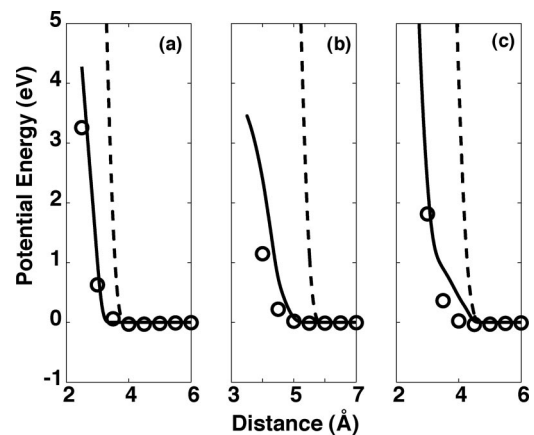


FIG. 2. Comparison of our modified pair potentials (solid lines) with the *ab initio* calculation (MP2/cc-aug-pVTZ) (circle) and the KTS (dashed lines) for three different configurations of a SiH_4 - SiH_4 interaction: (a), (b), and (c) represent the tail–tail, nose–nose, and the nose–tail configurations.

TABLE I. Modified Si:H interaction potential parameters. Units are kcal/mol and Å.

Two body [Eq. (3)]						
i - j	α	β	a	b	p	
Si-Si	352.477 814	11.603 192	2.0951 00	3.771 180	4	
H-H	804.959 233	0.044 067	3.9027 67	2.4	4	
Si-H	428.902 380	1.359 978	2.5378 84	3.2	4	
Three body [Eq. (4)]						
i - j - k	λ	μ	ν	$\gamma_{ij(k)}$	$\gamma_{ik(j)}$	χ
Si-Si-Si	166.666 667	6.000 000	9.000 000	2.514 120	2.514 120	3.771 180
H-H-H	230.605 452	0.132 587	-0.299 770	1.500 000	1.500 000	2.40
H-Si-H	100.633 157	7.200 000	10.800 000	2.212 406	2.212 406	3.20
Si-H-H	46.121 090	-2.939 390	1.800 000	0.558 821	3.328 492	2.70
Si-Si-H	17.110 500	12.000 000	18.000 000	1.848 715	2.539 432	3.00
Si-H-Si	1614.238 164	-0.400 000	-0.600 000	2.400 000	2.400 000	3.40

dominated by liquidlike characteristics, and the accuracy of the SW potential is known to increase with increasing particle size or temperature. The KTS potential energy V is a sum of two- and three-body interactions given by

$$V = \sum_{\substack{i,j \\ i < j}} V_2(i,j) + \sum_{\substack{i,j,k \\ i < j < k}} V_3(i,j,k),$$

where the two-body term is

$$V_2(r_{ij}) = \begin{cases} \alpha_{ij}(\beta_{ij}r_{ij}^{-p} - 1)\exp[a_{ij}/(r_{ij} - b_{ij})], & r_{ij} < b_{ij} \\ 0, & r_{ij} \geq b_{ij} \end{cases} \quad (3)$$

and the three-body term is

$$V_3(r_{ij}, r_{jk}, r_{ki}) = h(r_{ij}, r_{ik}, \theta_{jik}) + h(r_{jk}, r_{ji}, \theta_{ijk}) + h(r_{ki}, r_{kj}, \theta_{jki}), \quad (4)$$

where h is

$$h(r_{ij}, r_{ik}, \theta_{jik}) = \begin{cases} \lambda_{jik}(1 + \mu_{jik} \cos \theta_{jik} + \nu_{jik} \cos^2 \theta_{jik}) \exp\left[\frac{\gamma_{ij(k)}}{r_{ij} - \chi_{jik}} + \frac{\gamma_{ik(j)}}{r_{ik} - \chi_{jik}}\right], & \text{if } r_{ij} < \chi_{jik} \text{ and } r_{ik} < \chi_{jik}, \\ 0, & \text{otherwise.} \end{cases}$$

r is the distance between a pair of atoms, b_{ij} and χ_{jik} are the cutoff distance of the two-body and the three-body potentials, respectively, and θ_{jik} is the vertex angle at j subtended by i and k . α_{ij} , β_{ij} , p , and a_{ij} are fixed parameters chosen by Stillinger and Webber¹⁷ for the liquid silicon condition. Parameters λ_{jik} , μ_{jik} , ν_{jik} , $\gamma_{ij(k)}$, and $\gamma_{ik(j)}$ are constants formulated by Kohen, Tully, and Stillinger.¹⁸

In order to check if the KTS potential could describe the behavior of two interacting coated silicon nanoparticles accurately, we use SiH₄ to represent the smallest possible hydrogen-passivated silicon system. The KTS potential energy was computed at various distances r between the two silane molecules. For this interaction three different configurations were assessed: (a) three hydrogen atoms from each silane interacting symmetrically (tail-tail), (b) one hydrogen atom of each silane interacting symmetrically (nose-nose), and (c) nose-to-tail interaction. These results were then compared with an *ab initio* electronic structure calculation using the Gaussian program suite at the MP2/cc-aug-pVTZ level of theory (MP2 denotes the second-order Møller-Plesset pertur-

bation theory;²⁹ cc-aug-pVTZ is Dunning's triple correlation consistent basis sets with diffuse functions³⁰).

Figure 2 shows the results for the three configurations considered. It can be seen that the repulsive part of the KTS potential develops more than 1 Å farther out than the electronic structure calculation. The stronger H-H repulsion of the KTS potential would tend to make coated particles less reactive than the electronic structure calculation would suggest. Since this issue is at the crux of our investigation, we felt it was necessary to reparametrize a part of the KTS potential model. The new parameters were fitted to the electronic structure calculation using a genetic algorithm to optimize the parameters³¹ with constraints so as not to lose the important aspects of the KTS model. The final adjusted set of parameters for the modified KTS potential are summarized in Table I, and the corresponding plot of the energy surface is shown as a solid line in Fig. 2.

The bond distances, angles, and energies for the four silicon hydride molecules employed as input are shown in Table II. In general the results are quite reasonable; however, in order to get the KTS H-H repulsion to be less severe, it was

TABLE II. Molecular data from experiment and from the numerical models.

Molecule	Energy (kcal/mol)			Bond length (Å)			Angle (deg)		
	Expt.	KTS	This work	Expt.	KTS	This work	Expt.	KTS	This work
SiH ₄	302.8 ^a	302.50	290.99	1.48 ^d	1.470	1.510	109.47 ^d	109.47	109.40
SiH ₃	214.0 ^b	222.73	216.13	1.48 ^d	1.471	1.513	111.2 ^e	106.31	109.40
SiH ₂	144.4 ^c	145.06	142.62	1.48	1.474	1.517	92.4 ^e	102.61	109.40
Si ₂ H ₆	500.1 ^{f,g}	500.10	483.22						
Si-Si				2.331 ^d	2.325	2.329			
Si-H				1.492 ^d	1.470	1.510			
Si-Si-H							110.3 ^d	112.2	110.0
H-Si-Si							108.6 ^d	106.6	109.5

^aBased on enthalpy of formation given in Ref. 32.

^bBased on enthalpy of formation given in Ref. 33.

^cBased on enthalpy of formation given in Ref. 34.

^dReference 35.

^eReference 18.

^fReference 36.

^gReference 37.

necessary to reduce the cutoff distance from 2.8 to 2.4 Å. The result has little effect on the silane radicals (SiH₃ and SiH₂), but because of the lower H-H repulsion the potential makes the silane molecule too stable. Fortunately for our purposes, the surface-coated structures will look more like a combination of SiH and SiH₂ surface structures. The essential result is a compromise situation. Our feeling is that for this study it was more important to get the H-H repulsive interaction reasonably correct, since it will eventually be the bottleneck for particle–particle reactions.

III. SIMULATION PROCEDURE

All simulations were run on a Cray T3E computer running up to 64 processors. The trajectories of all the atoms are determined by integrating the equation of motion according to the velocity form of the Verlet algorithm³⁸ with rescaling of atomic velocities at each time step to achieve temperature control. A time step of 0.05 fs was typically used to ensure energy conservation, and the Verlet neighbor list with parallel architecture was employed in all the simulations. The neighbor list was renewed every 10 steps. The simulations take place in a spherical cavity of 20 nm radius with an elastic boundary condition.

The first step in the equilibration process was to prepare pure silicon particles of various sizes (200, 800, 1600, and 6400 atoms) at 300 K. After the angular momentum was removed, the particle temperature was raised to 2100 K using constant-temperature MD for 1 ns. Particle temperatures were reduced slowly to 300 K and equilibrated for 50 ps. The next step was to coat the particles with hydrogen atoms. Since the particles were already equilibrated, almost all surface atoms had a coordination number of three. A hydrogen atom was placed on each surface silicon atom at a distance of 1.5 Å and the particle temperature was maintained at 300 K for 10 ps. Any hydrogen atoms that were released from the surface were removed from the simulation, and the dynamics

repeated for 10 ps. After generating the hydrogen monolayer on the silicon particles, the temperature of the particles was slowly raised to the desired temperatures of 600, 1000, 1200, 1500, and 1800 K and maintained at constant temperature for 50 ps. For the last step in the preparation process, the simulations were switched to a constant-energy calculation for 20 ps. If the average temperature of the particle deviated by more than 10 K over this period, the equilibration process was repeated until the particle temperature deviated by less than 10 K.

To study particle–particle interactions, the particles were replicated and separated by a distance of 6 Å, so that the particles did not experience any interaction. Particles were then given a net specified velocity relative to the center of mass of the system so that they collided with zero impact parameter.

IV. RESULTS AND DISCUSSION

It is known that when solid particles interact at low velocity, the particle loses kinetic energy through elastic deformation, and the higher the collision energy, the higher the deformation, and the greater the resulting adhesion. However, at very high collision energies there is dissipation of kinetic energy into deformation, and any remaining energy that cannot be accommodated into the surface is converted into the kinetic energy of the rebound. If this rebound energy is greater than the adhesive energy, particles will not adhere to each other. On the other hand, liquid drops are more able to accommodate the kinetic energy into mechanical deformation, and for this reason liquid drops do not bounce off each other. However, in the latter case, the presumption is that the surfaces are mutually attractive. In the present study we investigate the dynamics of these interaction if the surfaces are mutually repulsive.

Figures 3(a) and 3(b) show an external and cross-section view of a nanoparticle consisting of 6400 silicon atoms,

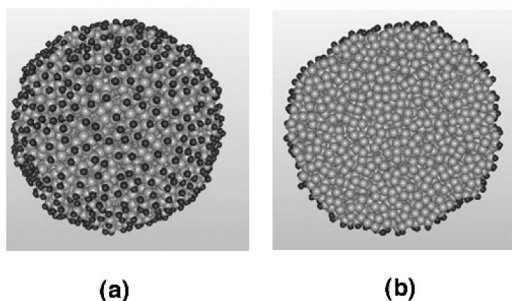


FIG. 3. A 6-nm hydrogen-coated silicon nanoparticle (6400 silicon+785 hydrogen atoms): (a) external view, (b) cross-section view.

coated with 785 hydrogen atoms, which corresponds to roughly a 6-nm particle. In none of our studies did hydrogen diffuse interior to the particle. In order to study the effect of the hydrogen-passivation layer on the reactivity of silicon nanoparticles, we have estimated the critical approach energy needed for reaction. The critical approach energies are obtained for various particle sizes (200 Si+74 H, 800 Si+211 H, 1600 Si+372 H, and 6400 Si+785 H atoms) at various initial temperatures (600, 1000, 1200, 1500, and 1800 K). The results are summarized in Fig. 4. The horizontal axis is the ratio of the approach energy KE_{app} (in terms of temperature) to the particle temperature T_p , and the vertical axis is the number of silicon atoms in a particle to the $\frac{4}{9}$ th power. The $\frac{4}{9}$ th power term, as one may recall, was the dependence obtained for the contact area when two spherical bodies approach each other. The dashed line at $KE_{app}/T_p = 1$ refers to the thermal collision case.

Clearly from the figure we see that the critical approach energy for reaction, for the cases where all silicon bonds are hydrogen saturated, are much higher than the particle thermal collision energy. We point out that an unpassivated particle (i.e., bare silicon) does not require any activation for a reactive collision. Furthermore, liquid drops are never known not to coalesce, because the driving force is the reduction in surface free energy. For nanometer-sized particles, individual atom-atom collisions dominate the collision force,³⁹ and in our study, the collision force should be dominated by the

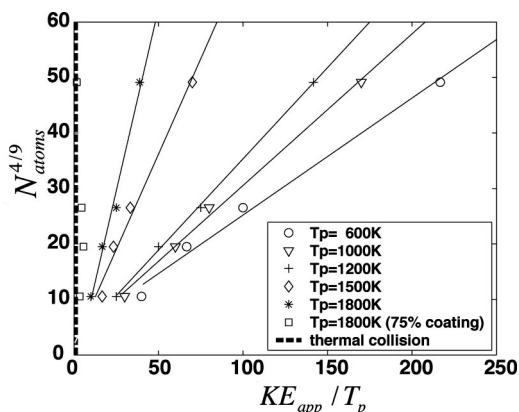


FIG. 4. Critical approach energy needed for reaction for various particle sizes and temperatures.

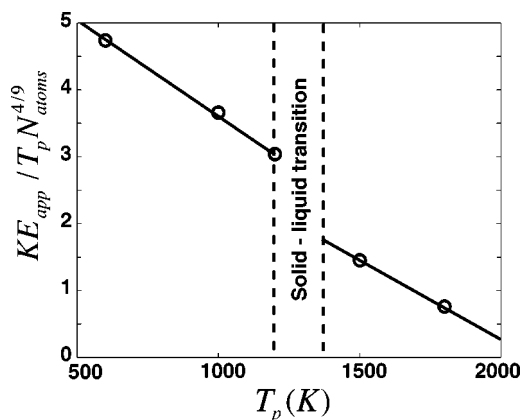


FIG. 5. Relationship between particle temperature and the reduced critical energy per unit contact area, $(KE_{app}/T_p)/N^{4/9}$.

repulsive interaction between hydrogen atoms on the surface of the particles. As a result, high collision energies are required to overcome the repulsive barrier. The most interestingly obvious result is that liquid particles bounce when collided at thermal energies. For example, we see that for a particle at 1800 K, coalescence occurs, depending on particle size, only at collision energies 8–30 times the thermal temperature of the particle. The critical approach energy increases with increasing particle size for all particle temperatures studied. Furthermore, the linear nature of the graphical results indicate consistency with the $\frac{4}{9}$ th power dependence for the interaction area. The latter result is a natural consequence of the contact surfaces, which are coated with hydrogen, producing a repulsive force between the particles, so that the critical approach energy must increase with increasing particle size.

It is also clear that hotter particles require a lower critical cluster kinetic energy for reaction. Furthermore this dependence becomes increasing pronounced as the particles get larger. This is more effectively presented by plotting the inverse of the slope (in Fig. 4) versus the particle temperature in Fig. 5. The physical meaning of such a plot is that the y axis represents the reduced critical collision energy per unit contact area. As the temperature is increased for solid particles a linear decrease in the reduced critical energy is seen. When the particles melt, the reduced critical energy transitions to a lower threshold value. This implies that when liquidlike, the internal kinetic motion of the atoms couple more effectively during a collision process.

The sensitivity of the role of the hydrogen repulsion is illustrated with particle collisions for a system in which particles have only 75% of the available surface sites covered with hydrogen. When compared to the saturated case, we see (in Fig. 4) that particle reactivity is significantly greater, but still requires a nonthermal collision for reaction to occur. In general, these particles do not show any size dependence on reactivity over the size range studied. In that regard they behave similar to unpassivated particles, but still require superthermal activation.

The hotter the particle, the lower the relative kinetic energy needed to induce particle-particle reaction. Even so, all reactive events required collision energies (at least for par-

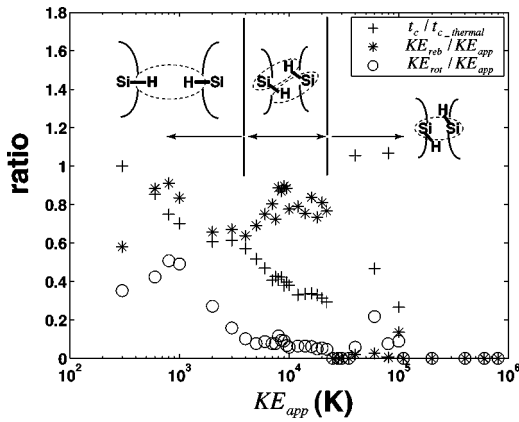


FIG. 6. Energy partitioning and normalized collision time, resulting from collision at various approach energies (200 Si + 74 H atoms, each) at 300 K.

ticles up to 1800 K) that were significantly above thermal energies.

To assess the role of energy transfer, we plot in Fig. 6 the ratio of (1) the particle collision period t_c to the period of the thermal collision case, (2) the kinetic energy of the rebound (translation only) to that of the approach, and (3) the kinetic energy of rotation to that of the approach for a particle at 300 K (200 Si + 74 H atoms) as a function of approach energy. The horizontal axis is the approach energy in terms of temperature (K). As expected we see that the collision period decreases as the approach energy increases for energies below 22 000 K. Between 800 and 4000 K, the ratio of the rebound energy to the approach energy also decreases with increasing approach energy. At higher energies we see this ratio goes to zero, corresponding to a reactive collision. We also note that at low collision energies a significant fraction of energy can be carried away as rotational energy, which is associated with the time available for the particles to deform during the collision. We will continue to refer to this figure in this paper as we explore in more detail the nature of these collisions.

Figures 7(a)–(c) show the temporal history of the poten-

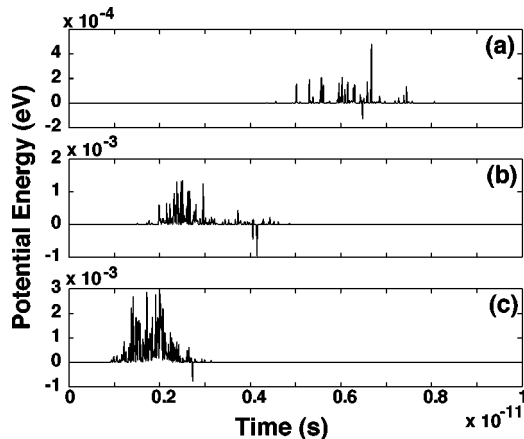


FIG. 7. Temporal history of the potential energy between two particles (200 Si + 74 H atoms, each) for (a) $KE_{app} = 300$ K, (b) $KE_{app} = 3000$ K, and (c) $KE_{app} = 10\,000$ K.

tial energy between two particles for approach energies of $KE_{app} = 300, 3000,$ and $10\,000$ K. Positive and negative interaction energies refer to repulsive and attractive energies, respectively. However, for these collisions we observe only sharp short-lived repulsive energies. These repulsive interactions result directly from individual H-H interactions. Since the mobility of hydrogen atoms is much higher than either that of silicon atoms or the whole particle, the hydrogen atoms at low collision energies are able to, on the time scale of the collision, move away from each other on the silicon surface atoms. At these approach energies (< 5000 K), we never observe any hydrogen atoms hopping to neighboring silicon surface atoms. In general, then, at the approach energies shown here, there are only H-H interactions between the particles, and a rough correlation can be seen between the collision period and the rebound energy ratio. We demark this boundary of interaction in Fig. 6 for clarity.

At higher collision energies, $KE_{app} > 5000$ K, we observe in Fig. 7 that like the low-temperature collisions these are mostly repulsive interactions. However, we see a much more complex long-lived interaction at these higher collision energies, with progressively more intense repulsive interactions. These repulsive energies are produced from both H-H and Si-H interactions (see Fig. 6). It seems that the appearance of such additional repulsive energy interactions increase the rebound energy of the particles, which breaks the proportionality between the collision period and the rebound energy ratio observed in Fig. 6 at lower collision energies.

It can be noticed from Fig. 6 that a relatively large amount of energy is transferred to rotation, which is usually not considered in micron-sized particles. This kind of energy transfer occurs partly because the surface being considered at the atomic scale is not smooth, and partly because the particles are not perfectly spherical. We noted that the ratio of the rotational energy to the approach energy decreases as the collision period decreases. Moreover, the rate of decrease of both the collision period and the rotational energy ratio are similar when $800\text{ K} < KE_{app} < 4000\text{ K}$. However, when $KE_{app} > 5000\text{ K}$, the ratio of the rotational energy to the approach energy stays constant at around 8.

It is also instructive to observe the number and type of interactions during the collision period for the three cases discussed above, as seen in Fig. 8. Here we observe that the interactions are much more long lived for the smaller collision energies, and that on the scales shown in Fig. 7 are not observable due to the small interaction energy when particles are not close enough. As the collision energy increases, the number of interactions increases and is more narrowly peaked in time. At low collision energies the interactions are primarily made up of H-H interactions, while the higher energies are equally split between Si-H and H-H interactions.

The adhesion of two particles can be observed at $24\,000\text{ K} < KE_{app} < 35\,000\text{ K}$ (see Fig. 6). At this range of KE_{app} the particles make a Si-Si bond between the particles right after the collision, following which particle coalescence begins. However, at still higher energies $40\,000\text{ K} < KE_{app} < 100\,000\text{ K}$, particle bounce can be observed even after making a Si-Si bond between the particles. Figure 9 again shows the temporal behavior of the potential energy of inter-

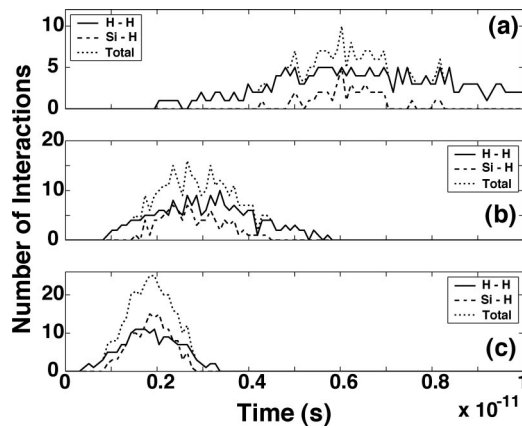


FIG. 8. Temporal behavior of the number and type of atomic interactions between two particles (200 Si+74 H atoms, each) for (a) $KE_{app}=300$ K, (b) $KE_{app}=3000$ K, and (c) $KE_{app}=10\,000$ K.

action (produced between two particles), but in this case for what seems like an initially reactive collision. We observe the presence of a large attractive energy of 2 eV after the collision, associated with a Si-Si bond between the particles. The repulsive contributions seen in the lower-energy collisions are also presented but do not show up in the scale of the graph presented. About 1 ps after the collision, the combination of the Si-Si, Si-H, and H-H repulsive contributions becomes too large to keep forming the Si-Si bond so that after 1.5 ps the particles break the Si-Si bond and bounce. This bouncing process makes the collision period long (i.e., $t_c/t_{c\,thermal}=1.06$ and 1.07 at $KE_{app}=40\,000$ and $80\,000$ K) and consumes a major part of the collision energy as a result of breaking the Si-Si bond. As a result the rebound energy becomes extremely small, e.g., $KE_{reb}/KE_{app}=0.03$ at $KE_{app}=40\,000$ K. At still higher energies $100\,000 < KE_{app} < 500\,000$ K, the particles form multiple Si-Si bonds and thereafter stick.

It is interesting to note in Fig. 6 that under some conditions the kinetic energies of the particle increase after collision, i.e., $KE_{reb} + KE_{rot} > KE_{app}$. At 800 K, for example, the total kinetic energy after collision is 40% higher. Figure 10 shows the temporal history of the potential energy during

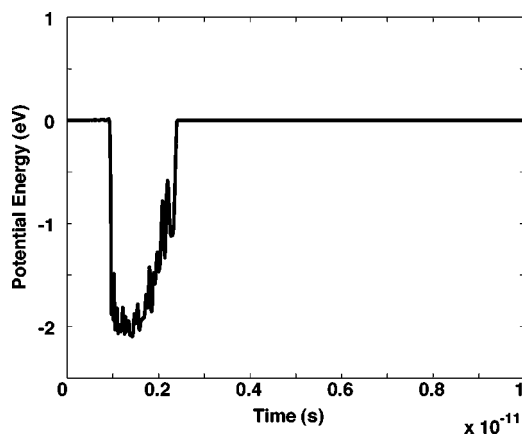


FIG. 9. Temporal dependence of the potential energy between two particles (200 Si+74 H atoms, each) at $KE_{app}=40\,000$ K.

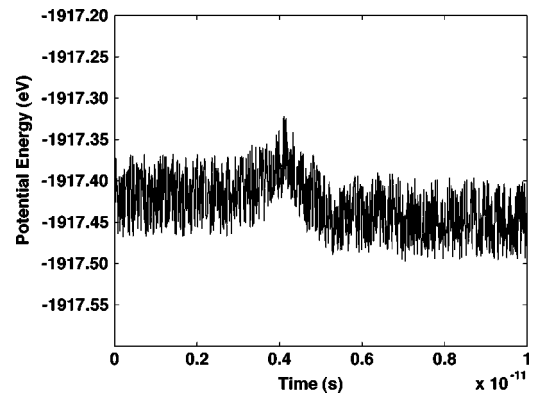


FIG. 10. Temporal dependence of the potential energy of two particles (200 Si+74 H atoms, each) for $KE_{app}=800$ K.

this collision. As the particles approach, the repulsive contributions result in deformation of the particle and an increase in the potential energy. Thereafter, the potential energy drops as the particles bounce, due to the recovery of the spherical shape and a reduction in surface area. However, the resulting particles have an energy that is lower by 0.03 eV and implies that the particles have cooled as a result of collision. This result is in contrast to elastic collisions that satisfy the condition $KE_{reb} + KE_{rot} < KE_{app}$, that is to say, particles leave with less kinetic energy after collision. However, the presence of the hydrogen passivation layer in our case removes the adhesion energy contribution, and at least for small particles, we have the possibility of having such “superelastic” collisions, $KE_{reb} + KE_{rot} > KE_{app}$.

The previous discussions focused on solidlike particles. We now turn our attention to liquid nanodrops, where we have raised the temperature of the particles to 1800 K. The first point we note is that the superelastic behavior observed is even more enhanced under liquid drop conditions. We found, for example, that for a 2000-K approach energy the drop kinetic energy after collision was 3.7 times larger [i.e., $(KE_{reb} + KE_{rot})/KE_{app}=3.7$]. Figures 11 and 12 show the temporal history of the kinetic and potential energy for such a collision. It is clear that the exit kinetic energy is significantly higher and corresponds to the decrease seen in the

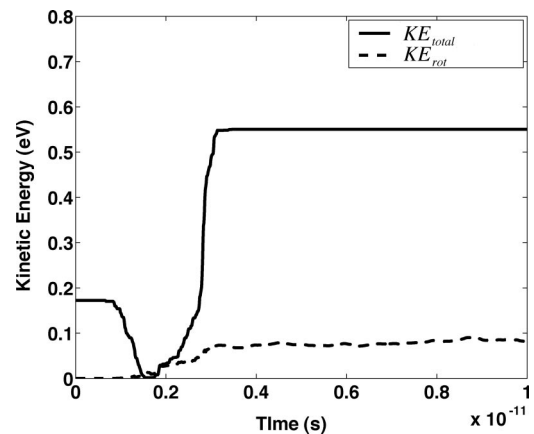


FIG. 11. Temporal dependence of the kinetic energy for a collision for (200 Si+74 H atoms, each), $KE_{app}=2000$ K.

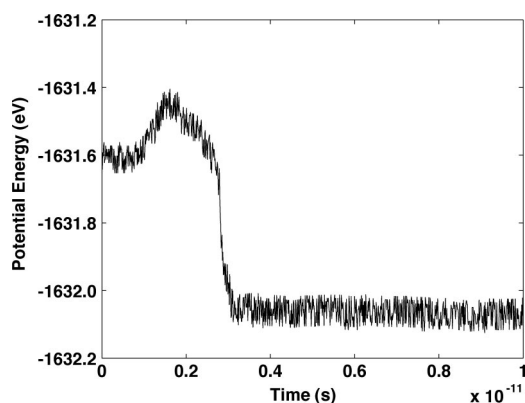


FIG. 12. Temporal dependence of the potential energy of two particles for (200 Si + 74 H atoms, each), $KE_{app} = 2000$ K.

potential energy. In this case, the increase in the rebound energy is 0.461 eV.

The contrast between solid and liquid during collision seen by plotting the reduced moment of inertia (a value of unity is a sphere) are shown in Fig. 13. Particles at 300 K maintain their spherical shapes and the contact area is small. On the other hand, the liquid drops at 1800 K deform in shape, thereby increasing the contact area and repulsive contribution, which leads to these superelastic collisions.

V. CONCLUSION

In this work we report on the use of constant-energy molecular dynamics simulations to investigate the effect of hydrogen-surface passivation of silicon nanoparticles on the reactivity to each other. The objective of the work was to determine if one could significantly alter nanoparticle reactivity during aerosol formation of silicon. In these simulations particles containing up to 6400 silicon atoms were studied at temperatures from 300 to 1800 K. In this work we have also reparametrized the Kohen-Tully-Stillinger empirical interatomic potential in order to obtain a more accurate representation of the H-H repulsive interaction.

It was found that the hydrogen-passivation layer prevents particle reaction at thermal collisions for all particle sizes and temperatures studied, including liquid nanodroplets. The critical approach energies for reaction were found for various sizes and temperatures. The general trend was that the critical collision energy increases with increasing particle size, due to an increase in the contact area between the colliding particles. On the other hand, the critical approach energy

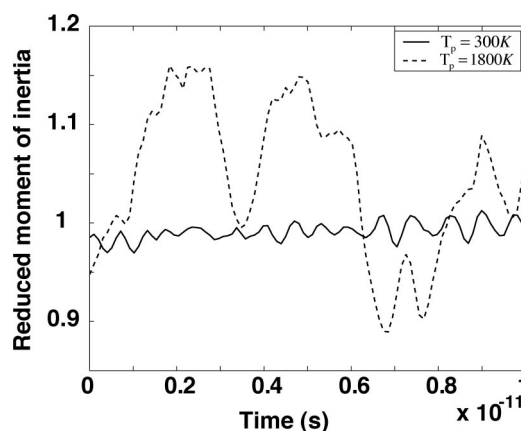


FIG. 13. Temporal dependence of the reduced moment of inertia during collision (200 Si + 74 H atoms, each).

decreases with increasing particle temperature due to increase of the reactivity of the surface atoms.

One of the most interesting findings was the effect of the passivation layer on the reactivity of liquid droplets. During aerosol growth of nanoparticles it is a standard assumption that liquid droplets are always reactive and subsequent coalescence is fast. These results show that the hydrogen monolayer provides an essentially perfect passivation layer.

Dynamic analysis of the results showed that the particle rebound energy decreases with decreasing collision period when only H-H interactions dominate, but become more complex at higher collision energies when both Si-H and H-H interactions contribute. Moreover, superelastic collisions were observed, wherein the $KE_{reb} + KE_{rot} > KE_{app}$, and internal cooling of the particles took place. The essence of this problem is a competition between the repulsive effect due to the passivation layer and the attractive effect of the Si-Si interaction, which depends on temperature, size, and contact area. The results of this paper indicate that surface passivation might be a very effective strategy to control the growth and morphology of nanoparticles grown from vapor.

ACKNOWLEDGMENTS

This work was supported by NSF Grant No. CTS-0083062, the Army High Performance Computing Research Center (DAAD19-01-2-0014), and the Army Durint Center for NanoEnergetics Research. The authors also wish to thank Nate Schultz for help on the *ab initio* calculations.

*Author to whom correspondence should be addressed. Corresponding address: 111 Church St. S.E., University of Minnesota, Minneapolis, Minnesota 55455. Electronic address: mrz@me.umn.edu

¹W. Koch and S. K. Friedlander, *J. Colloid Interface Sci.* **140**, 419 (1990).

²Y. Xiong and S. E. Pratsinis, *J. Aerosol Sci.* **24**, 283 (1993).

³S. H. Ehrman, S. K. Friedlander, and M. R. Zachariah, *J. Aerosol Sci.* **29**, 687 (1998).

⁴R. S. Windeler, K. E. J. Lehtinen, and S. K. Friedlander, *Aerosol Sci. Technol.* **27**, 174 (1997).

⁵R. S. Windeler, K. E. J. Lehtinen, and S. K. Friedlander, *Aerosol Sci. Technol.* **27**, 191 (1997).

⁶P. Biswas, G. Yang, and M. R. Zachariah, *Combust. Sci. Technol.* **134**, 183 (1998).

⁷S. K. Friedlander and M. K. Wu, *Phys. Rev. B* **49**, 3622 (1994).

⁸J. Frenkel, *J. Phys.* **9**, 385 (1945).

⁹M. R. Zachariah and M. J. Carrier, *J. Aerosol Sci.* **30**, 1139

- (1999).
- ¹⁰S. Ramalingam, D. Maroudas, and E. S. Aydil, *J. Appl. Phys.* **84**, 3895 (1998).
- ¹¹T. Ohira, O. Ukai, and M. Noda, *Surf. Sci.* **458**, 216 (2000).
- ¹²A. A. Onischuk, V. P. Strunin, M. A. Ushakova, and V. N. Panfilov, *Phys. Status Solidi B* **186**, 43 (1994).
- ¹³A. A. Onischuk, V. P. Strunin, M. A. Ushakova, R. I. Samoilo, and V. N. Panfilov, *Phys. Status Solidi B* **193**, 25 (1996).
- ¹⁴A. A. Onischuk, V. P. Strunin, M. A. Ushakova, and V. N. Panfilov, *J. Aerosol Sci.* **28**, 207 (1997).
- ¹⁵H. Hertz, *Miscellaneous Papers* (Macmillan, London, 1896), p. 146.
- ¹⁶K. L. Johnson, K. Kendall, and A. D. Roberts, *Proc. R. Soc. London, Ser. A* **324**, 301 (1971).
- ¹⁷F. H. Stillinger and T. S. Weber, *Phys. Rev. B* **31**, 5262 (1985).
- ¹⁸D. Kohen, J. C. Tully, and F. H. Stillinger, *Surf. Sci.* **397**, 225 (1998).
- ¹⁹M. V. R. Murty and H. A. Atwater, *Phys. Rev. B* **51**, 4889 (1995).
- ²⁰T. Ohira, O. Ukai, T. Adachi, Y. Takeuchi, and M. Murata, *Phys. Rev. B* **52**, 8283 (1995).
- ²¹T. Ohira, O. Ukai, M. Noda, T. Adachi, Y. Takeuchi, M. Murata, and H. Yoshida, *Mater. Res. Soc. Symp. Proc.* **336**, 177 (1994).
- ²²J. Tersoff, *Phys. Rev. Lett.* **56**, 632 (1986).
- ²³J. Tersoff, *Phys. Rev. B* **37**, 6991 (1988).
- ²⁴J. Tersoff, *Phys. Rev. B* **38**, 9902 (1988).
- ²⁵J. Tersoff, *Phys. Rev. B* **39**, 5566 (1989).
- ²⁶K. J. Raghavachari, *J. Chem. Phys.* **83**, 3520 (1985).
- ²⁷K. J. Raghavachari, *J. Chem. Phys.* **84**, 5672 (1986).
- ²⁸H. Balmane, T. Halicioglu, and T. A. Tiller, *Phys. Rev. B* **46**, 2250 (1992).
- ²⁹J. A. Pople, J. S. Binkley, and R. Seeger, *Int. J. Quantum Chem., Symp.* **10**, 1 (1976).
- ³⁰R. A. Kendall, T. H. Dunning, and R. J. Harrison, *J. Chem. Phys.* **96**, 6796 (1992).
- ³¹D. L. Carroll, Fortran genetic algorithm driver, <http://cuaerospace.com/carroll/ga.html>
- ³²M. W. Chase, Jr., C. A. Davies, J. R. Downey, Jr., D. J. Frurip, R. A. McDonald, and A. N. Syverud, *J. Phys. Chem. Ref. Data Suppl.* **14**, (1) (1985).
- ³³J. Doncaster and Walsh, *Int. J. Chem. Kinet.* **13**, 503 (1981).
- ³⁴J. Berkowitz, J. P. Green, H. Cho, and B. Ruscic, *J. Chem. Phys.* **86**, 1235 (1987).
- ³⁵*Gmelin Handbook of Inorganic and Organometallic Chemistry, Silicon Supplement B1* (Springer, New York, 1982).
- ³⁶S. G. Lias, T. E. Bartmess, J. F. Liebman, J. L. Holmes, R. D. Levin, and W. G. Mallard, *J. Phys. Chem. Ref. Data* **17**, Suppl. 1 (1998).
- ³⁷J. B. Pedley and J. Rylance, *Computer Analyzed Thermochemical Data: Organic and Organometallic Compounds* (University of Sussex, Brighton, UK, 1977).
- ³⁸L. Verlet, *Phys. Rev.* **159**, 98 (1967).
- ³⁹J. G. Gay and B. J. Berne, *J. Colloid Interface Sci.* **109**, 90 (1986).